Performance of an Interleaved Spread Spectrum OFDM System over Multipath Fading Channels

Pingzhou Tu[1], **Xiaojing Huang**[2], and **Eryk Dutkiewicz**[3], Non-members

ABSTRACT

In this paper we propose an interleaved spread spectrum orthogonal frequency division multiplexing (ISS-OFDM) system and investigate its performance over frequency selective multipath fading channels. The purpose is to exploit frequency diversity capability, develop an efficient spectrum spreading algorithm and improve the system performance over frequency selective multipath fading channels. At transmitter, a spectrum spread ISS-OFDM signal is generated by employing OFDM modulation and interleaving techniques. At the receiver, two solutions including serial demodulation and parallel demodulation for diversity combing are proposed, in which the received signals are combined by using a maximum ratio combining (MRC) technique. The simulation indicates that higher frequency diversity is achieved, and the Bit Error Rate (BER) and Peak-to-Average Power Ratio (PAR) performances of the proposed ISS-OFDM system over frequency selective multipath fading channels are improved significantly as compared with the conventional OFDM systems. Another unique characteristic is that the spectrum spreading factor and diversity order provided by the system are reconfigurable to achieve cognitive communications.

Keywords: Diversity, Interleaving, Spread spectrum, OFDM, Fading channels

1. INTRODUCTION

Frequency selective fading is a dominant impairment in wireless communications. The channel fading reduces received signal-to-noise ratio (SNR) and degrades the bit error rate (BER). It also causes channel delay spread and introduces inter-symbol interferences (ISI) [1]. To combat the frequency selective fading in wireless communications, diversity techniques must be resilient [2]. Orthogonal frequency division multiplexing (OFDM) technique as one of the multi-carrier transmission techniques has extended the symbol duration and effectively reduced the ISI by inserting a cyclic prefix, which is greater than the channel delays, before the signal is transmitted to the channel [3;4]. However, its diversity potentials have not been fully exploited yet.

Driven by OFDM applications against channel fading and by enabling multipath diversity, some different forms of OFDM systems with different diversity techniques have been proposed, such as the multiple-input multiple-output OFDM (MIMO-OFDM) systems [5], the frequency diversity OFDM (FD-OFDM or adaptive AFD-OFDM) systems [6-9], and the spread-spectrum multiple-carrier multiple-access (SS-MC-MA) [10]. Among these systems, the MIMO-OFDM is one of the most typical ones. It adopts a very commonly used method for achieving spatial diversity by employing multiple antennas at both ends of wireless links. It holds the potential to drastically improve the spectral efficiency and link reliability in future wireless communications systems, and is regarded as a particularly promising candidate for next-generation fixed and mobile wireless systems. However, one major problem for MIMO-OFDM systems is that the scalability of the diversity is very limited. The other two methods, FD-OFDM and SS-MC-MA, use the same way of multiplying the transmitted data stream by an orthogonal spreading code before modulation in order to achieve frequency diversity. The spectrum spreading is accomplished by putting the same data on all parallel subcarriers, producing a spreading factor equal to the number of subcarriers. Although these systems enable full multipath diversity, they need a large number of side information transmissions, which causes considerable rate loss [11;12].

In this paper we propose a method for achieving frequency diversity and the corresponding receiver algorithms for diversity combining. The proposed system is called the interleaved spread spectrum orthogonal frequency division multiplexing (ISS-OFDM) system. In this system, frequency diversity is enabled by spread spectrum modulation and interleaving [13-15] techniques, rather than using multiple antennas, orthogonal codes, or other side information. At the transmitter, each data symbol modulates the corresponding subcarriers multiple times, and several replicas bearing the same data information can be obtained. The replicas of the same data information are interleaved sequentially and then transmitted in different time slots, instead of being added together.

Manuscript received on June 25, 2007 ; revised on June 24, 2008.

[1,2,3] The authors are with School of Electrical, Computer and Telecommunication Engineering, University of Wollongong, Australia., E-mail: pt01@uow.edu.au, huang@uow.edu.au and eryk@uow.edu.au

The interleaving operation results in signal spectrum being expanded into multiple subbands, each of which contains the same data information, so that frequency diversity is achieved. After frequency selective channel fading, the receiver can collect signal energy from several signal subbands by using maximal ratio combining (MRC) techniques. Thus, the probability that all signal components fade simultaneously is reduced considerably, leading to great system performance such as BER improvement [16-18].

With the increase of frequency diversity, another performance improvement brought about is that the peak-to-average power ratio (PAR) performance of ISS-OFDM system is reduced dramatically. As is well known, one of the main disadvantages in conventional OFDM system is the large PAR of the transmitted signal [19;20], due to the addition of the modulated signals by using Inverse Fast Fourier Transform (IDFT) operation. In ISS-OFDM system, since the information bearing subcarriers are interleaved instead of superimposed, the PAR of the transmitted signal is reduced significantly. Meanwhile, the number of the total samples in one ISS-OFDM symbol increases greatly, which results in reduced signal power spectrum density if the total signal energy remains unchanged.

The paper is organized as follows. First, the system model is described in section 2. Then, the OFDM signal generation process with both time diversity and frequency diversity is described in section 3, and the signal diversity characteristics are analyzed in the frequency domain and time domain. In section 4, the corresponding two receiver models are proposed. Section 5 is devoted to system performance simulation and discussion, in which the system average bit error probability and computational complexity are given. Finally, conclusions are drawn in section 6.

2. SYSTEM MODEL

As is well known, when signals are propagated in a frequency selective multipath fading channel, the presence of reflecting objects and scatters in the channel creates a constantly changing environment that dissipates the signal energy in amplitude, phases and time. These effects result in multiple versions of the transmitted signal, which are received by the receiver at different times from different multipaths, displaced with respect to one another in time and spatial orientation.

Fig.1 displays the ISS-OFDM baseband model. We assume that the channel is frequency selective with slow fading, and the noise is additive white Gaussian noise (AWGN) with zero mean. The data bit to symbol mapping scheme can be any of M-ary modulation. To demonstrate the system performance improvement, in this paper we take only quadrature phase shift keying (QPSK) as the mapping method to simulate the generation of ISS-OFDM signal and compare the system performance. A cyclic prefix (CP) is also added to preserve the orthogonality of the subcarriers and eliminate intersymbol interference (ISI) between consecutive ISS-OFDM symbols.

We now illustrate the function of each module showed in Fig. 1. The function of the transmitter is to generate an ISS-OFDM signal with time and frequency diversities. The complex QPSK data symbols to be transmitted are first divided into an N by 1 vector, where N is the number of subcarriers. This vector modulate N subcarries in parallel by using the complex exponential spreading (CES) technique, and then the spread signals are interleaved to form an ISS-OFDM symbol of N^2 samples. After a cyclic prefix insertion and filtering, the ISS-OFDM signal $y(m)$ (also represented by $Y(k)$ in the frequency domain) with spectrum spreading is transmitted into the frequency selective multipath fading channel with impulse response $h(m)$ (denoted as $H(k)$ in the frequency domain). Meanwhile, the AWGN noise $v(m)$ (denoted as $V(k)$ in the frequency domain) is added to the signal. After being distorted by the fading channel, the signal is filtered and CP removed, and then demodulated. The output of the demodulator is equalized and combined to form a decision variable U_k by employing maximal ratio combining (MRC) technique.

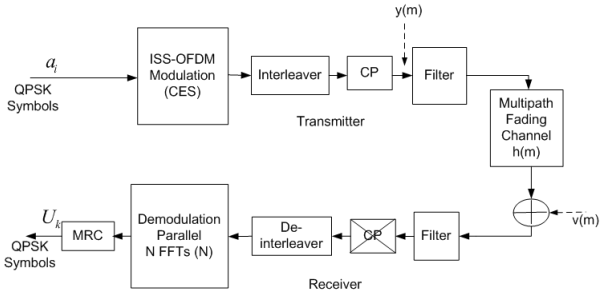

Fig.1: *Baseband system model*

We assume that the transmitted ISS-OFDM signal bandwidth $B_{ISS-OFDM}$ is greater than the coherence bandwidth $(\Delta f)_c$, $B_{ISS-OFDM} \gg (\Delta f)_c$ thus the channel can be considered as a frequency-selective fading channel. The channel model can be expressed in the form

$$h(m) = \sum_{i=0}^{N^2-1} \alpha_i(m)\delta(m - m_i)$$

where $\alpha_i(m)$ is the multipath fading channel attenuation factor on the m^{th} path and m_i is the propagation delay for the m^{th} path. Correspondingly, the channel frequency response is written as

$$H(k) = \sum_{m=0}^{N^2-1} h(m)e^{-j\frac{2\pi}{N^2}km}. \quad (1)$$

After the transmitted signal, denoted as $y(m)$, passes through the fading channel, the received equivalent low-pass signal is viewed as the convolution between $h(m)$ and $y(m)$ plus noise as follows

$$r(m) = h(m) \bigotimes y(m) + v(m) \tag{2}$$

where $v(m)$ represents the complex-valued white Gaussian noise process corrupting the signal. In frequency domain, Equation (2) is equivalent to the output of the DFT demodulator.

$$R(k) = H(k) \cdot Y(k) + V(k) \tag{3}$$

where $R(k), Y(k), H(k)$ and $V(k)$ denote the frequency representations of the received signal $r(m)$, the transmitted signal $y(m)$ the channel impulse response $h(m)$ and the noise $v(m)$, respectively.

3. DIVERSITY IN ISS-OFDM SIGNALS

3.1 Transmitter Model

Fig. 2 shows the transmitter model, which indicates the generation process of ISS-OFDM signal with time diversity and frequency diversity. Let $a_i (i = 0, 1, \cdots, N)$ denotes the i^{th} complex-valued symbol of the N QPSK symbols to be transmitted. The N QPSK symbols are modulated by the CES modulator, and then interleaved by the interleaver to form the ISS-OFDM signal with time diversity and frequency diversity. Time diversity is achieved by CES modulation and frequency diversity is obtained by interleaving.

3.2 Time Diversity of ISS-OFDM Signals

After serial to parallel conversion the $N \times 1$ parallel QPSK symbols modulate the corresponding N subcarriers. If the ISS-OFDM symbol period is T_s, $f_i = \frac{i}{T_s}$ denotes the i^{th} subcarrier frequency of the N orthogonal subcarriers, and a_i modulates the i^{th} subcarrier at time $t = \frac{n}{N} T_s$, $n = 0, 1, \cdots, N-1$, where is the sampling time index. The modulated symbol on the i^{th} subcarrier and the n^{th} time instant is written as follows,

$$y_i(n) = a_i e^{j2\pi f_i t} = a_i e^{j2\pi ni/N}. \tag{4}$$

In the ISS-OFDM symbol duration T_s, each element of the $N \times 1$ data symbol vector modulates the same corresponding subcarrier N times, so that N elements in the vector generate an $N \times N$ sample matrix after modulation. In consequence, N replicas of each data symbol are produced in symbol duration T_s by CES modulation, and the time diversity of the ISS-OFDM symbol is achieved. Fig. 3 displays the process of achieving time diversity in the ISS-OFDM system with subcarrier number $N = 4$.

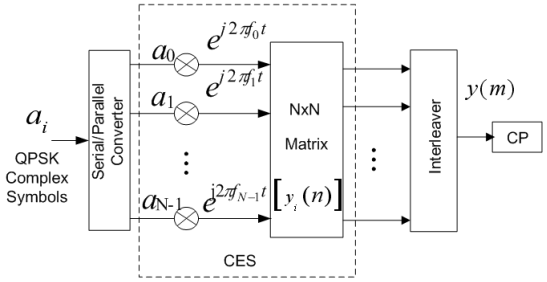

Fig.2: *Transmitter model*

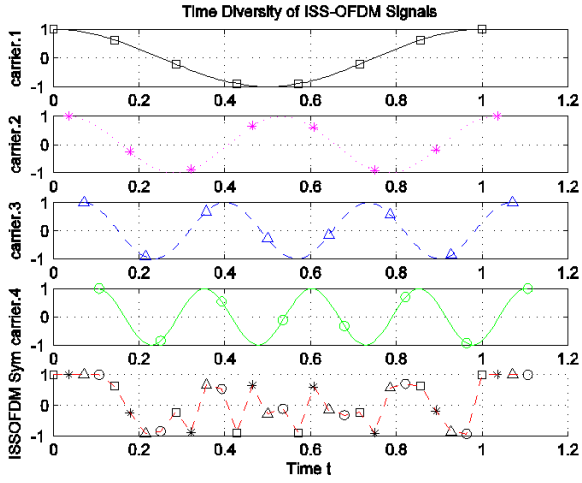

Fig.3: *Time diversity of ISS-OFDM signals with subcarrier number N=4*

Mathematically, the matrix can be expressed as

$$[y_i(n)] = \begin{pmatrix} y_0(0), y_0(1), \cdots, y_0(N-1) \\ y_1(0), y_1(1), \cdots, y_1(N-1) \\ \cdots \\ y_{N-1}(0), y_{N-1}(1), \cdots, y_{N-1}(N-1) \end{pmatrix}$$
$$= \begin{pmatrix} a_0 e^{j2\pi 0*0/N}, a_0 e^{j2\pi 0*1/N}, \cdots, a_0 e^{j2\pi 0*(N-1)/N} \\ a_1 e^{j2\pi 0*0/N}, a_1 e^{j2\pi 0*1/N}, \cdots, a_1 e^{j2\pi 0*(N-1)/N} \\ \cdots \\ a_{N-1} e^{j2\pi 0*0/N}, a_{N-1} e^{j2\pi 0*1/N}, \cdots, a_{N-1} e^{j2\pi 0*(N-1)/N} \end{pmatrix} \tag{5}$$

Let W_N^{-ni}, where $W_N = e^{-j\frac{2\pi}{N}}$, denote the i^{th} sub-carrier at the $\frac{n}{N} T_s$ time instant, and

$$Diag(a_i) = \begin{pmatrix} a_0, 0, \ldots 0 \\ 0, a_0, 0 \ldots 0 \\ \ldots\ldots\ldots\ldots \\ 0, 0, \ldots a_{N-1} \end{pmatrix}.$$

Thus, Equation (5) can be rewritten as,

$$\begin{pmatrix} a_0 W_N^{-0*0}, a_0 W_N^{-0*1}, \ldots, a_0 W_N^{-0*(N-1)} \\ a_1 W_N^{-1*0}, a_1 W_N^{-1*1}, \ldots, a_1 W_N^{-1*(N-1)} \\ \cdots \\ a_{N-1} W_N^{-(N-1)*0}, a_{N-1} W_N^{-(N-1)*1}, \ldots, a_{N-1} W_N^{-(N-1)*(N-1)} \end{pmatrix}$$

$$= Diag(a_i) \times \left[W_N^{ni}\right]. \quad (6)$$

Equation (6) indicates one way of implementing CES modulation, by which the N transmitted data symbols at the input of the modulator are rearranged into the diagonal elements of a diagonal matrix. Since the input signal of the modulator is in the form of a diagonal matrix, the output signal is an $N \times N$ sample matrix as denoted in Equation (5).

3.3 Frequency Diversity of ISS-OFDM Signals

After CES modulation, the $N \times N$ samples are shifted in time and placed on different time slots to form a serial sequence of length N^2 in the time domain. This operation is a process of interleaving. Here, different interleaving algorithms can be employed such as pseudo random interleaving, periodic interleaving and convolutional interleaving. In the following, we discuss the periodic interleaving process. The periodic interleaving can be realized by shifting N modulated subcarriers on different time slots and adding them together. For instance, the i^{th} subcarrier of the N subcarriers is shift by $i \cdot \tau$, where τ is the time interval, $\tau = \frac{T_s}{N^2}$, then, the N shifted subcarriers are interleaved to form one ISS-OFDM symbol with N^2 samples. The m^{th} sample in the ISS-OFDM symbol, denoted by $y(m)$, $m = nN + i = 0, 1, \cdots, N^2 - 1$, can be mathematically written as follows,

$$y(m) = \sum_{i=1}^{N} \sum_{n}^{N} y_i(n) \delta\left[m - i - nN\right],$$

where $\delta\left[m - nN - i\right] = \begin{cases} 1, for\ m & = & nN + i \\ 0, for\ m & \neq & nN + i. \end{cases}$ is the unit impulse. Expressing $m = nN + i, y(m)$, can be simplified in the form

$$\begin{aligned} y(m) &= y(nN + i) \\ &= y_i(n). \end{aligned} \quad (7)$$

The mathematical equations above can be interpreted as follows. All N samples in a column of the $N \times N$ matrix are taken out from the $N \times N$ matrix, shifted in time, and then placed in different time slots, instead of being superimposed together as in conventional OFDM systems. Due to the shifting in time for each sample, the phase of each subcarrier is shifted. In the frequency domain, the signal spectrum is expanded to N subbands, each of which contains N orthogonal subcarriers modulated by the same transmitted data symbols. Therefore, the ISS-OFDM signal's frequency diversity is obtained. Fig. 4 displays the spectrum of ISS-OFDM signals with subcarrier number $N = 4$. It is seen that the modulated data symbol on the i^{th}(in this case $i = 1, 2, 3, 4$) subcarrier appears in all $N = 4$ subbands.

The frequency domain representation of the ISS-OFDM signal can be obtained by taking discrete Fourier transform (DFT) of the signal in the time domain.

$$\begin{aligned} Y(k) &= DFT(y(m)) \\ &= DFT(y(nN + i)) \\ &= \sum_{nN+i=0}^{N^2-1} y(NN + i) e^{-j\frac{2\pi}{n^2}(nN+i)k}. \end{aligned}$$

That is,

$$Y(k) = \sum_{n=0}^{N-1} \sum_{i=0}^{N-1} y(nN + i) e^{-j\frac{2\pi}{N^2}(nN+i)k}. \quad (8)$$

Substituting $y(nN + i)$ from Equation (7) into Equation (8), we have

$$Y(k) = \sum_{n=0}^{N-1} \sum_{i=0}^{N-1} y_i(n) e^{-j\frac{2\pi}{N^2}(nN+i)k}. \quad (9)$$

Substituting $y_i(n)$ from Equation (4) into Equation (9) yields

$$\begin{aligned} Y(k) &= \sum_{n=0}^{N-1} \sum_{i=0}^{N-1} a_i e^{j\frac{2\pi}{N}ni} e^{-j\frac{2\pi}{N^2}(nN+i)k} \\ &= N \sum_{i=0}^{N-1} a_i e^{j\frac{2\pi}{N}ki} \underbrace{\frac{1}{N} \sum_{n=0}^{N-1} e^{-j\frac{2\pi}{N}(k-i)n}}_{\delta((k-i)_N}. \end{aligned}$$

That is

$$Y(k) = N \sum_{i=0}^{n-1} a_i e^{-j\frac{2\pi}{N^2}ki} \delta((k - i)_N), \quad (10)$$

where

$$\delta((k - i)_N) \begin{cases} 0, & k & \neq & pN + i \\ 1, & k & = & pN + i \end{cases}.$$

Equation (10) can be also rewritten as

$$Y(pN+i) = N a_i e^{-j\frac{2\pi}{N^2}(pN+i)i}, p = 0, 1, \cdots, N-1. \quad (11)$$

Equation (11) indicates that each data symbol a_i is modulated on the i^{th} subcarrier in every subband, and the signal spectrum is spread N times. The spectrum spread signal contains N subbands and each of which bears the same information. Fig. 4 shows the spectrum of the ISS-OFDM signal with subcarriers number $N = 4$. It shows that the ISS-OFDM signal contains 4 subbands, each subband carries the same information. The order of frequency diversity achieved is 4.

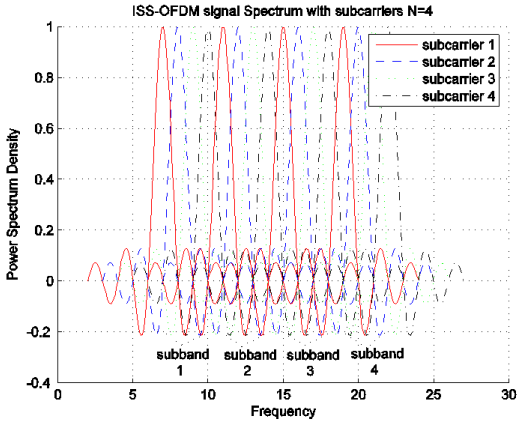

Fig.4: *Spectrum of ISS-OFDM symbol with subcarrier number* $N = 4$.

4. DIVERSITY COMBINING OF ISS-OFDM SIGNALS

At the receiver, the received signal is firstly filtered by using a root raised cosine filter. The filter is matched to the transmitter filter, so that the overall effect of filtering is that of a raised cosine filtering. The passband of the receiver filter is designed to be flexibly reconfigurable according to the system requirements. One or more subbands of received signal can be selected through the receiver filter. Assuming that all the N subbands of the received signal are passed through the filter, the diversity combining can be implemented in two receiver solutions. One is the serial demodulation mode; the other one is parallel demodulation mode.

4.1 Diversity Combining in Solution I: Serial Demodulation

4.1.1 Frequency Domain Representation of Received Signals in Serial Demodulation Mode

Fig. 5 shows the receiver structure of solution I, which is realized by using one DFT operation of size N^2. After CP remove and DFT demodulation, the output of the demodulator is equalized, and then combined by maximal ratio combining (MRC) technique.

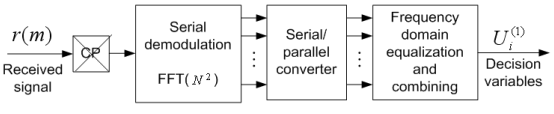

Fig.5: *Serial demodulation and combination*

Substitute $Y(k)$ from Equation (10) into Equation (3), the received diversity signal at the input of the receiver in the frequency domain is rewritten as follows

$$R(k) = N \sum_{i=0}^{N-1} a_i \delta((k-i)_N) e^{-j\frac{2\pi}{N^2}ki} H(k) + V(k), \quad (12)$$

where $k = 0, 1, \cdots, N^2 - 1$.

According to Equation (12), the output of the serial demodulation is as follows

$$R(pN + i) = N a_i C_{i,p}^{(1)} + V(pN + i), \quad (13)$$

where

$$\begin{aligned} C_{i,p}^{(1)} &= e^{-j\frac{2\pi}{N^2}(pN+i)i} H(pN + i), \\ p &= 0, 1, \cdots, N-1, \quad i = 0, 1, \cdots, N-1. \end{aligned}$$

It can be observed from Equation (13) that $R(pN+i)$ can be decomposed into N groups. Each group forms one subband which consists of subcarriers, and each subcarrier consists of N the corresponding weighted signal and noise. Generally, we assume that the received signal contains M subbands, $M \leq N$, and use the M subbands to demodulate the transmitted signal. The structure of $R(pN + i)$ can be illustrated in Fig. 6.

The transmitted data symbol a_i, $i = 0, 1, \cdots, N-1$, can be recovered from $R(pN+i)$, $p = 0, 1, \cdots, M-1$, which can be expressed in matrix form as follows:

$$\begin{pmatrix} R(i) \\ R(N+i) \\ \vdots \\ R((M-1)N+i) \end{pmatrix} = N \begin{pmatrix} C_{i,0}^{(1)} \\ C_{i,1}^{(1)} \\ \vdots \\ C_{i,M-1}^{(1)} \end{pmatrix} a_i + \begin{pmatrix} V(i) \\ V(N+i) \\ \vdots \\ V((M-1)N+i) \end{pmatrix}.$$

According to the above matrix equation, a minimum mean squared error (MMSE) estimate of a_i can be obtained as follows:

$$\hat{a}_i = \frac{1}{N} \left(\begin{pmatrix} C_{i,0}^{(1)*} & C_{i,1}^{(1)*} & \cdots & C_{i,M-1}^{(1)*} \end{pmatrix} \begin{pmatrix} C_{i,0}^{(1)} \\ C_{i,1}^{(1)} \\ \vdots \\ C_{i,M-1}^{(1)} \end{pmatrix} + \frac{1}{SNR} \right)^{-1} .$$

$$\begin{pmatrix} C_{i,0}^{(1)*} & C_{i,1}^{(1)*} & \cdots & C_{i,M-1}^{(1)*} \end{pmatrix} \begin{pmatrix} R(i) \\ R(N+i) \\ \vdots \\ R((M-1)N+i) \end{pmatrix}$$

$$= \frac{1}{N} \sum_{q=0}^{M-1} \frac{C_{i,q}^{(1)*}}{\sum_{p=0}^{M-1} \left| C_{i,p}^{(1)} \right|^2 + \frac{1}{SNR}} R(q+i),$$

where SNR is the signal-to-noise ratio before the MMSE equalization.

To analyze the system BER performance, the normalized MMSE can be expressed as

$$\varepsilon^2_{\min} = \left(SNR \begin{pmatrix} C^{(1)*}_{i,0} & C^{(1)*}_{i,1} & \cdots & C^{(1)*}_{i,M-1} \end{pmatrix} \begin{pmatrix} C^{(1)}_{i,0} \\ C^{(1)}_{i,1} \\ \vdots \\ C^{(1)}_{i,M-1} \end{pmatrix} + 1 \right)^{-1}$$

$$= \frac{1}{SNR \sum_{p=0}^{M-1} \left| C^{(1)}_{i,p} \right|^2 + 1}.$$

Therefore, the output signal-to-noise ratio after MMSE equalization is

$$\gamma_{out} = \frac{1-\varepsilon^2_{\min}}{\varepsilon^2_{\min}} = \frac{1}{\varepsilon^2_{\min}} - 1 SNR \sum_{p=0}^{M-1} \left| C^{(1)}_{i,p} \right|^2.$$

Assuming QPSK modulation for data symbols and making a Gaussian distribution approximation for the intersymbol interference after MMSE equalization, we finally obtain the expression for the average BER using the Q function

$$P_e^{(MMSE)} = E\left(Q\sqrt{\gamma_{out}}\right) \tag{14}$$

where $E(\cdot)$ denotes ensemble average over channel coefficients.

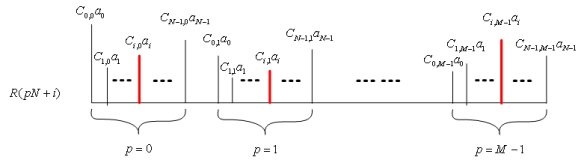

Fig.6: *The structure of $R(pN+i)$*

4.1.2 Diversity Combining

From Equation (13), we see that a data symbol a_i is transmitted on different subcarriers and experiences independent fading. Thus, another effective way to gain frequency diversity is to directly use the maximal ration combining (MRC) technique to collect signal energy from all information bearing subcariers. In this way the system diversity can be made full use of and the best system performance can be achieved.

Similar to the above MMSE equalization, we assume that only M subbands, $M \leq N$, are used to recover the transmitted data symbols. The MRC process proceeds as follows. First, we multiply the conjugated channel coefficient $C^{(1)*}_{i,p}$ with the received $R(pN+1)$ to compensate the channel phase shift and weight the information bearing subcarrier with a gain proportional to the signal strength. Then, all the weighted subcarriers corresponding to the same data symbol a are combined to produce the decision variable $U^{(1)}_i$ for the detection of a_i. That is,

$$U^{(1)}_i = \sum_{p=0}^{M-1} C^{(1)*}_{i,p} R(pN+i).$$

To analyze the BER performance of the MRC technique, we substitute $R(pN+i)$ in the above equation with Equation (13) and have

$$U^{(1)}_i = N \sum_{p=0}^{M-1} \left| C^{(1)}_{i,p} \right|^2 a_i + \sum_{p=0}^{M-1} C^{(1)*}_{i,p} V(pN+i).$$

The output signal-to-noise ratio after MRC can be obtained as

$$\begin{aligned} \gamma^{(1)} &= \frac{\left(N \sum_{p=0}^{M-1} \left| C^{(1)*}_{i,p} \right|^2 \right)^2 E\left(|a_i|^2 \right)}{E\left(\left| \sum_{p=0}^{M-1} C^{(1)*}_{i,p} V(pN+1) \right|^2 \right)} \\ &= \frac{\left(\sum_{p=o}^{M-1} \left| C^{(1)}_{i,p} \right|^2 \right)^2 N^2 E\left(|a_i|^2 \right)}{\sum_{p=0}^{M-1} \left| C^{(1)}_{i,p} \right|^2 E\left(|V(pN+i)|^2 \right)} \\ &= \sum_{p=0}^{M-1} \left| C^{(1)}_{i,p} \right|^2 SNR, \end{aligned}$$

where $SNR = \dfrac{N^2 E\left(|a_i|^2 \right)}{E\left(|V(pN+i)|^2 \right)}$ is the signal-to-noise ratio before MRC.

For QPSK modulated data symbols, the average error probability can be therefore written as:

$$P_e^{MRC} = E\left(Q\sqrt{\gamma^{(1)}} \right). \tag{15}$$

From Equation (14) and Equation (15) we see that the MMSE equation and the MRC have the same performance for the serial demodulation.

4.1.3 Diversity Performance

After normalization, SNR and E_b/N_0 have the relation $SNR = \frac{2}{M} \frac{E_b}{N_0}$ (Refer to Appendix), the system BER performance expression in Equation (15) can be rewritten as:

$$P_e^{(MRC)} = E\left(Q\left(\sqrt{\sum_{p=0}^{M-1}\left|C_{i,p}^{(1)}\right|^2 \frac{1}{M}\frac{E_b}{N_0}}\right)\right). \quad (16)$$

4.2 Solution II: Parallel Demodulation by DFT

The demodulation in Solution I using single DFT is straightforward to realize. However, the computational complexity in Solution I is relatively high.

In order to reduce the complexity, we propose Solution II, a parallel demodulation method by employing multiple DFTs. The parallel demodulation method consists of cyclic prefix removal, deinterleaver, demodulation, and maximum ratio combining. Compared with the serial demodulation, the difference is the number of DFTs employed. In the parallel DFT solution, the demodulation is realized by employing N DFTs of size N, rather than a single DFT of size N^2.

4.2.1 Frequency Domain Representation of Received Signals in Parallel Demodulation Mode

Fig. 7 shows the receiver structure for Solution II using parallel demodulation, which is realized by using N parallel DFTs, each of which is of size N . We assume that the signal in the time domain at the receiver input is known. To obtain the data vector for each DFT operation, the time domain signal is split into N groups, each group is demodulated by using an DFT operation with the size N .

In order to compensate the channel distortion using frequency domain equalization, we must find out the relationship among each parallel DFT output, the channel coefficient, and the transmitted data symbol. For doing that, the first step is to express the received signal in the time domain at the input of the receiver in terms of the channel frequency response and the transmitted data symbol.

The signal in the time domain at the input of the receiver can be obtained by conducting the inverse DFT (IDFT) of size N^2 on $R(k)$, i.e.,

$$r(m) = IDFT(R(k)) = \frac{1}{n^2}\sum_{k=0}^{N^2-1} R(k)e^{j\frac{2\pi}{N^2}km}. \quad (17)$$

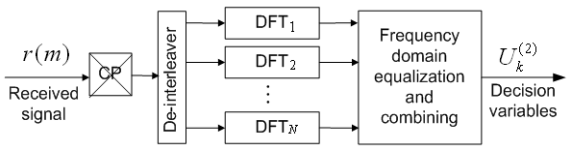

Fig.7: *Parallel demodulation and combination*

Substituting $R(k)$ from Equation (12) into Equation (17), the received signal in the time domain $r(m)$ can be rewritten as:

$$r(m) = \frac{1}{N}\sum_{k=0}^{N^2-1}\sum_{i=0}^{N-1} a_i e^{-j\frac{2\pi}{N^2}(i-m)}\delta((i-k)_N)H(k) + \frac{1}{N^2}\sum_{k=0}^{N^2-1} V(k)e^{j\frac{2\pi}{N^2}km} \quad (18)$$

After the time domain signal is received, it is then de-interleaved. The de-interleaved process is exactly the same as the method discussed in Solution I.

After de-interleaving, the signal in the time domain is split into N data streams, each of which can be demodulated using one DFT operation. Thus, to demodulate the $N \times N$ data samples simultaneously, parallel DFTs, each of size N, are needed. In this way, the demodulation of the received signal is completed by employing N parallel DFT operations. The deinterleaved signals can be written as:

$$r_i(n) = r(nN+i) = r(m), \quad \begin{aligned} i &= 0,1,\cdots,N-1, \\ n &= 0,1,\cdots,N-1, \end{aligned}$$

To derive the frequency domain representation of $r_i(n)$, we can perform the DFT operation on $r_i(n)$. The output of the demodulation can be obtained as follows:

$$\begin{aligned} R_i(k) &= \sum_{n=0}^{N-1} r_i(n)e^{-j\frac{2\pi}{N}kn} \\ &= \sum_{n=0}^{N-1} r(nN+i)e^{-j\frac{2\pi}{N}kn}. \end{aligned}$$

where $k = 0,1,\cdots,N-1$. It must be noted that the definition of k in the above equation is a different variable from that of $R(k)$ in Solution I, in which $k = 0,1,\cdots,N^2-1$.

Substituting $r(m)$ in Equation (18) in to the above equation, $R_i(k)$ can be written as follows:

$$R_i(k) = \frac{1}{N}\sum_{n=0}^{N-1}\left[\sum_{k'=0}^{NN-1}\sum_{i'=0}^{N-1} a_i e^{-j\frac{2\pi}{NN}k'(i'-nN-i)} \delta((k'-i,)_N)H(k') + \frac{1}{N}\sum_{k'=0}^{NN-1} V(k') e^{j\frac{2\pi}{NN}k'(nN+i)}\right] e^{j\frac{2\pi}{N}kn}$$

$$= \sum_{k'=0}^{N-1}\sum_{i'=0}^{N-1} a^i \cdot e^{j\frac{2\pi}{NN}k'(i-i')}\delta((i'-k')_N)H(k')\frac{1}{N}$$
$$\underbrace{\frac{1}{N}\sum_{n=0}^{N-1} e^{j\frac{2\pi}{N}(k'-k)n}}_{\delta((k'-k)_N)} + \frac{1}{NN}\sum_{k'=0}^{NN-1} V(k')e^{j\frac{2\pi}{NN}k'i}$$
$$\underbrace{\frac{1}{N}\sum_{n=0}^{N-1} e^{j\frac{2\pi}{N}(k'-k)n}}_{\delta((k'-k)_N)}$$

Since $k'-k$ must be integer multiples of N, i.e., $k'-k=qN$, we express $k'=qN+k$, and $R_i(k)$ becomes

$$\begin{aligned} R_i(k) &= \sum_{i'=0}^{N-1} a_i \sum_{k'=0}^{NN-1} H(k')e^{j\frac{2\pi}{NN}k'(i-i')} \\ &\quad \cdot \delta((i'-k')_N)\underbrace{\delta((k'-k)_N)}_{k'=qN+k} \\ &+ \frac{1}{N}\sum_{k'=0}^{NN-1} V(k')\underbrace{\delta((k'-k)_N)}_{k'=qN+k}e^{j\frac{2\pi}{NN}k'i} \end{aligned}$$

$$= \sum_{i'=0}^{N-1} a_i \sum_{q=0}^{N-1} H(qN+k)e^{-j\frac{2\pi}{NN}(qN+i)(i'-i)}$$
$$\underbrace{\delta((qN+k-i')_N)}_{i'=k} + \frac{1}{N}\sum_{q=0}^{N-1} V(qN+k)e^{j\frac{2\pi}{NN}(qN+i)i}.$$

Again, since $qN+k-i'$ must be integer multiples of N, we have $i'=k$ and $R_i(k)$is finally expressed as

$$\begin{aligned} R_i(k) &= a_k\sum_{q=0}^{N-1} H(qN+k)e^{-j\frac{2\pi}{NN}(qN+i)(k-i)} \\ &\quad + \frac{1}{N}\sum_{q=0}^{N-1} V(qN+k)e^{j\frac{2\pi}{NN}(qN+k)i} \\ &= \underbrace{a_k\sum_{q=0}^{N-1} e^{j\frac{2\pi}{N}q(i-k)}H(qH+k)e^{-j\frac{2\pi}{NN}i(k-i)}}_{C_{k,j}^{(2)}} \\ &\quad + \underbrace{\frac{1}{N}\sum_{q=0}^{N-1} V(qn+k)e^{j\frac{2\pi}{NN}(qN+k)i}}_{v_{k,i}} \\ &= a_kC_{k,i}^{(2)} + v_{k,i}. \end{aligned} \quad (19)$$

Where $C_{k,i}^{(2)} = \sum_{q=0}^{N-1} e^{j\frac{2\pi}{N}(i-k)}H(qN+k)e^{-j\frac{2\pi}{NN}i(k-i)}$ is an equivalent channel coefficient and $v_{k,i} = \frac{1}{N}\sum_{q=0}^{N-1} V(qN+k)e^{j\frac{2\pi}{NN}(qN+k)i}$ is the independent additive noise.

Now the relationship among each demodulated output $R_i(k)$, the equivalent channel coefficient $C_{k,i}^{(2)}$, transmitted signal a_k, and noise $v_{k,i}$ is clearly shown in Equation (19).

4.2.2 Diversity Combining and Performance

The MRC technique for Solution II is very similar to the one used in Solution I. After the parallel DFTs, the decision variable $U_k^{(2)}$ for the detection of a_k is calculated by

$$U_k^2 = \sum_{i=0}^{N-1} C_{k,i}^{(2)*}R_i(k).$$

To analyze the BER performance of the MRC technique, we substitute $R_i(k)$ in the above equation with Equation (19) and have

$$U_k^{(2)} = \sum_{i=0}^{N-1}\left|C_{k,i}^2\right|^2 a_k + \sum_{i=0}^{N-1} C_{k,i}^{(2)*}v_{k,i}.$$

The output signal-to-noise ratio after MRC can be obtained as

$$\begin{aligned} \gamma^{(2)} &= \frac{\left(\sum_{i=0}^{N-1}\left|C_{k,i}^{(21)}\right|^2\right)^2 E\left(|a_k|^2\right)}{E\left(\left|\sum_{i=0}^{N-1} C_{k,i}^{(2)*}v_{k,i}\right|^2\right)} \\ &= \frac{\left(\sum_{i=0}^{N-1}\left|C_{k,i}^{(2)}\right|^2\right)^2 E\left(|a_k|^2\right)}{\sum_{i=0}^{N-1}\left|C_{k,i}^{(21)}\right|^2 E\left(|v_k|^2\right)} \\ &= \sum_{i=0}^{N-1}\left|C_{k,i}^{(2)}\right|^2 SNR, \end{aligned}$$

where $SNR = \frac{E\left(|a_k|^2\right)}{E\left(|v_{k,i}|^2\right)}$ is the signal-to-noise ratio before MRC.

Similar to Solution I, the average error probability can be written as:

$$P_e^{(MRC)} = E\left(Q\sqrt{\gamma^{(2)}}\right). \quad (20)$$

5. SYSTEM PERFORMANCE

5.1 PAR Performance and Analysis

Assume that the number of subcarriers $N=32$, and the data symbol mapping scheme uses QPSK.

The use of the other mapping methods would leads to different relation between SNR and E_b/N_0. Consequently, the system BER performance would be different, but the total trend would keep unchanged.

After the modulation, an $N \times N$ matrix is formed, the modulated subcarriers in the matrix are interleaved and placed on different time slots to form a serial sequence. The sequence is pulse shaped by passing through a root raised cosine filter and thus an ISS-OFDM signal $y(t)$ is generated. The PAR of $y(t)$ can be written as

$$\xi = \frac{\max\left[|y(t)|^2\right]}{E\left[|y(t|^2)\right]}, \tag{21}$$

where max[·] is the maximum instantaneous power of the ISS-OFDM signal and $E[\cdot]$ is the expected value.

The generated ISS-OFDM signal has N^2 samples and contains N subbands, each of which contains N subcarriers and carries the same data information. The transmitter is designed so that M subbands are selected, $M = 0, 1, \cdots, N$ respectively, and thus the transmitted signal contains M subbands. To observe the PAR performance, we select the signal bandwidth with $M = 1, 2, 4, 8, 16$ and 32 subbands respectively (M is the spreading factor), and the filtered signal is oversampled by a factor of four, which is commonly used to estimate the PAR of an analogy signal from its samples. The actual PAR of the continuous-time signal can not be determined by using Nyquist sampling rate. In order to evaluate the PAR performance of the transmitted signal, the signal should be oversampled by a factor of four, which is sufficient to produce accurate PAR [23].

According to Equation (21), we can compute the PAR performance curves as shown in Fig. 8 shows the ISS-OFDM transmitted signal PAR performance when PAR exceeds a certain threshold PAR0 with the increase of the spectrum spreading factor M from 1 to 32.

It can be seen from Fig. 8 that with the increase of the number of subbands, the PAR performance is improved considerably. The most right-hand-side curve shows the PAR performance of ISS-OFDM signal when M is equal to 1, in this case, the ISS-OFDM signal is in fact a conventional OFDM signal.

As M increases to 2, 4, 8, 16, and 32 respectively, the PAR gains are 0.5dB, 1.5 dB, 3.5 dB, 5 dB and 7 dB respectively. Therefore, the PAR of the ISS-OFDM signal is greatly reduced compared to PAR of the conventional OFDM signal.

5.2 Diversity Scalability

A distinct feature in the ISS-OFDM system is the signal diversity scalability. Since the signal spectrum is very wide and contains N subbands, each of which contains the same data information, any one or more subbands can be used to demodulate the transmitted

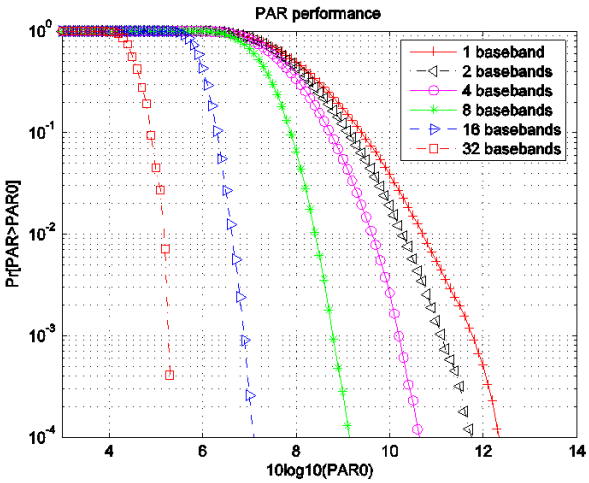

Fig.8: *PAR performance for ISS-OFDM signals Compared to the conventional OFDM*

information according to the system requirement and channel condition. At the transmitter, if we configure the transmitter filter so that the signal spectrum is spread M times, $M \leq N$, where L is the length of multipath channels, the system frequency diversity order would be M. We assume that the number of the subcarriers of the ISS-OFDM is N, then the maximum spectrum spread factor is and the maximum diversity capability of the ISS-OFDM system is N. The more the diversity capability is provided by the system, the better BER performance the system can achieve. But if the diversity capability provided by the system is more than the channel multipath L, the extra diversity capability provided by the system is redundant. That is to say, if $M > L$, the diversity of the ISS-OFDM system is limited to the channel multipath length , which is shown in Fig. 9

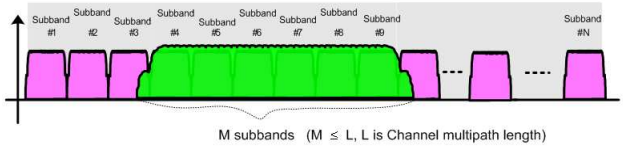

Fig.9: *Diversity scalability*

The scalability performance of diversity has a range of applications. One of the potential applications is to be applied to dynamic spectrum-sharing management system for the efficient and effective utilization of the spectrum. If there are one or more subbands interfered, the system can jump to the other non-interfering subbands to complete communications and the interfered frequency subbands can be easily avoided. For some unlicensed users in some spectrum subbands, the system can adapt its system frequency to the spectrum holes detected by spectrum scanning devices. As indicated in Fig.10, the system

can realize communications by avoiding interference bands or by using some spectrum holes. These features of ISS-OFDM system are agreeable to the notion of adaptive spectrum managements of cognitive radio communications [21;22].

5.3 BER Performance

In Equation (16) and Equation (20), we derived the BER performance (conditional error probability) of the ISS-OFDM system when the ISS-OFDM transmitted signal $y(t)$ contains N subbands. When only M out of subbands of the signal $y(t)$ are used for system transmission, the system BER performance can be achieved and compared with the conventional OFDM signal.

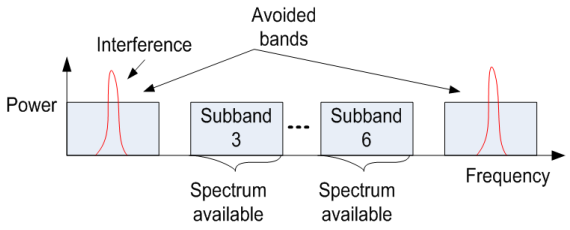

Fig.10: *Bandwidth reconfigurable system and efficient spectrum usage*

In order to verify the effectiveness of the system diversity in multipath fading channels, the BERs of the system are simulated according to Equation (20), the system performance is compared at the different conditions of the system transmission band without interference, with interference, and with interference removed. These BERs are shown in Fig. 11, Fig. 12 and Fig. 13, respectively.

Fig. 11 indicates the system BER performance with system transmission subband numbers $M = 2$, 4, 8, 16 and 32, and without interference. It is observed that with the increase of M, the system BER performance is improved considerably. After $M = 16$, a further increase of transmission subbands is not obviously beneficial to the improvement of the BER performance, but is helpful for interference avoidance.

Under the same conditions of system transmission subband numbers, the system BER with one subband interfered is shown in Fig. 12. The interference to noise ratio (INR) is 3dB. It is seen that the impact from the interference results in $5 \sim 6$ dB degradation at the BER performance of 10^{-6} compared with the system performance without interference.

As shown in Fig. 13 after the interfered subband is removed when $M = 4$, 8, 16 and 32, the system BER is improved by $0.5 \sim 5$ dB compared with the system

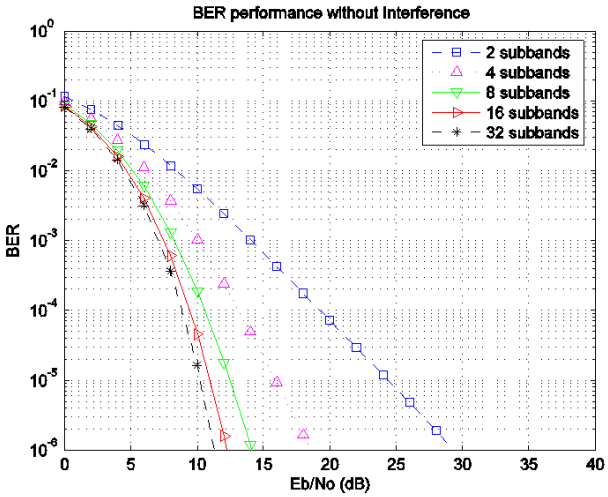

Fig.11: *BER performance without interferences in fading channels.*

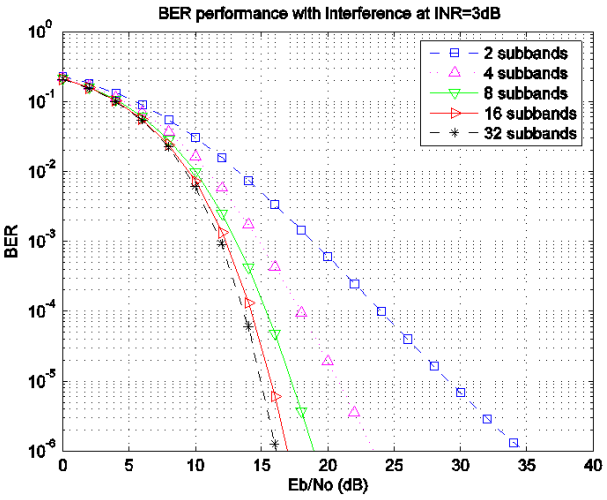

Fig.12: *BER performance with interferences in fading channels.*

5.4 Computational Complexity

Computational complexity for both solution I and solution II can be compared. Assumed the number of subcarriers is N and M subbands of the ISS-OFDM signal are received at receiver. For solution I, if we ignore the complex addition, one DFT operation in long size of $N \cdot M$ performs the demodulation, the total complex multiply is $\frac{1}{2}N \times M \log_2 NM$. For solution II, M DFT of size N operations are employed to complete demodulation, the total complex multiply is $\frac{1}{2}N \times M \log_2 N$.

The computational complexity in solution II is reduced $\frac{\log_2 NM}{\log_2 N}$ times than Solution I. In addition, due to the flexible reconfigurable bandwidth, the dynamic subband selection of ISS-OFDM system allows

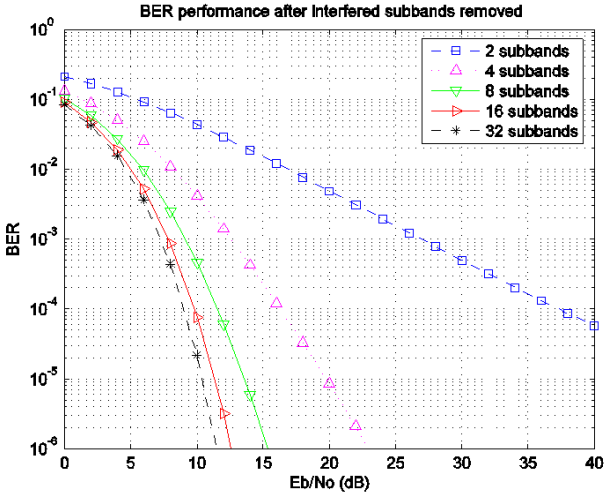

Fig.13: *BER performance after interfered subbands removed adaptively in fading channels.*

different systems working in the same allocated frequency band without interference. Other Performances, such as power efficiency, are also improved to some extent in ISS-OFDM system.

6. CONCLUSION

In this paper, we have investigated the diversity performance of an interleaved spread spectrum OFDM system including transmitter signal generation, two receiver solutions and system performance. The investigation shows that the combination of spread spectrum modulation and interleaving techniques is an efficient way of implementing spectrum spread and achieving frequency diversity. Since the spread spectrum modulation and interleaving techniques are jointly employed, the frequency diversity and time diversity are efficiently developed and utilized.

By investigating two receiver algorithms of serial demodulation and parallel demodulation methods, we showed that both two receiver algorithms can recover transmitted signal very well in terms of system BER performance, but the parallel demodulation in solution II can reduce the computational complexity greatly and its structure is flexible to be reconfigured. Parallel demodulation method is more preferable for the proposed system.

Compared to other previous spread spectrum OFDM, ISS-OFDM has superior performance in terms of system BER and PAR, reconfigurable structure, and flexible system bandwidth. It realizes spectrum spread by combination of spread spectrum modulation and interleaving techniques, rather than conventional frequency hopping or orthogonal spread code. It does not degrade the range of communications or need to transmit side information.

The proposed ISS-OFDM system can be used in ultra-wideband communications. It is also expected to be used in cognitive radio adaptive modulation techniques.

References

[1] J. G. Proakis, *Digital Communications*, 4 ed. New York, USA: Mc Graw Hill, 2000.

[2] R. Novak and W. A. Krzymien, "Diversity Combining Options for Spread Spectrum OFDM in Frequency Selective Channels," *Wireless Communications and Networking Conference*, vol. 1, pp. 308-314, 2005.

[3] M. Welborn, "Frequency Hoppers and FCC UWB Rules," *IEEE P802. 15 Wireless Personal Area Networks*, vol. IEEE P802.15-03/271r2 2003.

[4] A. Batra et al., "Multi-band OFDM Physical Layer Proposal Area Networks (WPANs)," *IEEE P802. 15-03/26r2, IEEE P802. 15 Wireless Perosnal Area Networks*, pp. 1-69, 2003.

[5] R. S. Blum, Y. Li, and J. H. Winters and Q. Yan, "Improved Space-Time Coding for MIMO-OFDM Wireless Communications," *IEEE Transactions on Communications*, vol. 49, no. 11, pp. 1873-1878, 2001.

[6] R. Novak and W.A.Krzymien, "SS-OFDM-F/TA System Packet Size and Structure for High Mobility Cellular Environments,", 2 ed 2003, pp. 1438-1444.

[7] J. Qaddour and D. Leonard, "Beyond 3G: Uplink Capacity Estimation for Wireless Spread-Spectrum Orthogonal Frequency Division Multiplexing (SS-OFDM)," *Global Telecommunications Conference*, vol. 7, pp. 4139-4141, 2003.

[8] S. W. Kim, K. H. Yoon, R. G. Jung, and J. W. Son and H. G. Ryu, "Adaptive Frequency Diversity OFDM (AFD-OFDM) Communication Narrow-Band," *Joint Conference of 10th Asia-Pacific Conference on Communications and 5th International Symposium on Multi-Dimensional Mobile Communicaitons*, vol. 1 and 2, pp. 834-838, 2004.

[9] R. Novak and W. A. Krzymien, "An Adaptive Downlink Spread Spectrum OFDM Packet Data System with Two-Dimensional Radio Resource Allocation: Performance in Low-Mobility Cellular Environments," *Wireless Personal Multimedia Communications, 2002. The 5th International Symposium on*, vol. 1, pp. 163-167, 2002.

[10] S. Kaiser and K. Fazel, "A Flexible Spread-Spectrum Multicarrier Multiple-Access System for Multi-Media Applications," *Personal, Indoor and Mobile Radio Communications*, vol. 1, pp. 100-104, 1997.

[11] G. J. Saulnier and Z. Ye and M. J. Medley, "Performance of a Spread Spectrum OFDM System in a Dispersive Fading Channel with Inter-

ference," *Military Communications Conference*, vol. 2, pp. 679-683, 1998.

[12] P. Xia and S. Zhou and G. B. Giannakis, "Bandwidth- and Power-Efficient Multicarrier Multiple Access," *IEEE Transactions on Communications*, vol. 51, no. 11, pp. 1828-1836, 2003.

[13] V. G. S. Prasad and K. V. S. Hari, "Interleaved Orthogonal Frequency Division Multiplexing System," *Acoustics, Speech, and Signal Processing,* vol. 3, p. III-2745-III-2748, 2002.

[14] P. Tu and X. Huang and E. Dutkiewiz, "A Novel Approach of Spread Spectrum in OFDM Systems," *International Symposium on Communications and Information Technologies, ISCIT '06*, pp. 487-491, 2006.

[15] A. D. S Jayalath and C. Tellambura, "Use of data permutation to reduce the peak-to-average power ratio of an OFDM signal," *Wireless Communications and Mobile Computing*, vol. 2, pp. 187-203, 2002.

[16] O. Edfors, M. Sandell, J. J. V. D. Beek, and S. K. Wilson and P. O. Borjesson, "OFDM Channel Estimation by Singular Value Decomposition," *IEEE Transactions on Communications*, vol. 46, no. 7, pp. 931-938, 1998.

[17] P. Xia and S. Zhou and G. B. Giannakis, "BER Minimized OFDM Systems with Channel Independent Precoders," *IEEE Transactions on Communications*, vol. 51, no. 11, pp. 1828-1836, 2003.

[18] L. Wan and V. K. Dubey, "BER Performance of OFDM system Over Frequency Nonselective Fast Ricean Fading Channels," *IEEE Transaction Letters*, vol. 5, no. 1, pp. 19-21, 2001.

[19] C. Schurgers and M. B. Srivastava, "A Systematic Approach to Peak-to-Average Power Ratio in OFDM," *Proc. SPIE*, vol. 4474, no. 11, pp. 454-464, 2001.

[20] S. B. Slimane, "Peak-to-Average Power Ratio Reduction of OFDM Signals Using Broadband Pulse Shaping," *http://citeseer. ist. psu. edu/438615. html*, pp. 889-893, 2002.

[21] S. Haykin, "Cognitive Radio: Brain-Empowered Wireless Communications," *IEEE Journal on Selected Areas in Communications*, vol. 23, no. 2, pp. 201-219, 2005.

[22] B. Ackland, D. Raychaudhuri, M. Bushnell, C. Rose, and I. Seskar, "High Performance Coginitive Radio Platform with Intergeated Physical and Network Layer Capabilities (Interim Technical Report)," WINLAB, Rutgers University,2005.

[23] A. D. S Jayalath and C. Tellambura, "Interleaved PC-OFDM to Reduce the Peak-to-average Power Ratio," *in Advanced Signal Processing for Communication Systems*, Springer, Netherlands, pp. 239-250, 2007.

Pingzhou Tu received the bachelor degree in computer science and applications from Harbin Engineering University, China, in 1991 and master degree in computer architecture from Huazhong University of Science and Technology, China, in 1999 and Ph.D degree from University of Wollongong, Australia, in 2008. From 1991 to 2004 he worked for Wuhan Marine Communication Research Institute China as an engineer and senior engineer in the fields of marine communications. He has completed lots of research and development projects on marine communications in the fields of wired and wireless communication. From 2005 to 2008 he was doing Ph.D in University of Wollongong. His current research interests include wireless communication networks, digital signal processing.

Xiaojing Huang was born in Hubei, China, on 3 October, 1963. He received his Bachelor of Engineering, Master of Engineering, and Ph.D. degrees from Shanghai Jiao Tong University, Shanghai, China, in 1983, 1986, and 1989, respectively, all in electronic engineering. From 1989 to 1994, he worked in the Electronic Engineering Department of Shanghai Jiao Tong University, where he had been a Lecturer since 1989 and an Associate Professor since 1991. Form 1994 to 1997, he was the Chief Engineer with Shanghai Yang Tian Science and Technology Co. Ltd., Shanghai, China. In 1998, he joined the Motorola Australian Research Centre, Botany, NSW, Australia, where he had been a Senior Research Engineer since 1999 and a Principal Research Engineer since 2003. Since 2004, he has been an Associate Professor in the School of Electrical, Computer and Telecommunications Engineering at the University of Wollongong, Wollongong, NSW, Australia. He also holds a number of visiting positions in Shanghai Jiao Tong University, Chinese Academy of Science, and the Commonwealth Scientific and Industrial Research Organisation. His research interests are in communications theory, digital signal processing, and wireless communications networks. He is a member of the Institute of Electrical and Electronics Engineers.

Eryk Dutkiewicz received his Bachelor of Engineering degree in Electrical and Electronic Engineering from the University of Adelaide in 1988, his Master of Science in Applied Mathematics degree from the University of Adelaide in 1992 and his PhD in Telecommunications from the University of Wollongong in 1996. From 1988 to 1992 he worked at the Overseas Telecommunications Corporations Research Labs in Sydney developing pioneering broadband multimedia telecommunications systems based on ATM networking. From 1992 to 1999 he worked at the University of Wollongong conducting research and teaching activities in the area of telecommunications and mobile networks. From 1999 to 2004 he worked at Motorola Labs in Sydney where he became the Manager of the WLAN Technologies Laboratory. The Laboratory conducted R&D of wireless technologies for Motorola's home networking, public safety and semiconductor products. From 1999 to 2004 he worked at Motorola Labs in Sydney where he became the Manager of the WLAN Technologies Laboratory. The Laboratory conducted R&D of wireless technologies for Motorola's home networking, public safety and semiconductor products. While with Motorola Labs he was an active member of the IEEE 802.11 standards organizations contributing to the successful WiFi standards. He is currently a Professorial Fellow at

the University of Wollongong in charge of the Wireless Technologies Laboratory. He has had research contracts in the area of next generation wireless technologies with Motorola Inc., USA, Agere Systems Ltd Australia and Freescale Semiconductor Inc, USA. Prof. Dutkiewicz holds visiting appointments at the Chinese Academy of Sciences in Beijing and at the Shanghai Jiao Tong University. His current research interests include Quality of Service in broadband wireless networks and optimization of wireless sensor networks.

APPENDIX

The relationship between SNR and E_b/N_0 depends on the symbol mapping mode. In this paper, we only consider this relationship based on QPSK mapping mode. In Solution I, according to Fig. 6,

$$SNR = \frac{\sigma_x^2}{\sigma_v^2} = \frac{MN\sigma_x^2}{MN\sigma_v^2} = \frac{MN\sigma_x^2 \cdot T \cdot MN}{MN\sigma_v^2 \cdot T \cdot MN} = \frac{E_s \cdot N}{MN\sigma_v^2 \cdot T \cdot MN} = \frac{E_s \cdot N}{N_0 \cdot \frac{1}{T} \cdot T \cdot MN} = \frac{2}{M}\frac{E_b}{N_0}.$$

Thus, the relationship between SNR and $\frac{E_b}{N_0}$ can be expressed as

$$SNR = \frac{2}{M}\frac{E_b}{N_0}.$$

This relationship between SNR and $\frac{E_b}{N_0}$ also applies to the Solution II.